



A method for improving the properties of famotidine

Yongfeng Zhao^a, Ying Fan^b, Yan Zhang^c, Hong Xu^d, Min Li^e, Yunjie Zhu^c,
Zhao Yang^{a,c,*}

^a College of Pharmacy, Qingdao University, Qingdao, 266071, China

^b Pharmacy Department, Qingdao Special Servicemen Recuperation Center of CPLA Navy, Qingdao, 266071, China

^c Qingdao Institute for Food and Drug Control, Qingdao, 266073, China

^d Shandong University of Science and Technology, Qingdao, 266590, China

^e Anqiu People's Hospital, Weifang, 262199, China

ARTICLE INFO

Keywords:

Famotidine
M-nitrobenzoic acid
Crystal structure
Aqueous solubility
Permeability

ABSTRACT

According to crystal engineering, the pharmaceutical intermediate *m*-nitrobenzoic acid (MNBA), which contains a carboxylic acid group, was selected as a cofomer (CCF) for drug cocrystallization with famotidine (FMT), and a new stable FMT salt cocrystal was synthesized. The salt cocrystals were characterized by scanning electron microscopy, differential scanning calorimetry, thermogravimetric analysis, infrared spectroscopy, powder X-ray diffraction and X-ray single crystal diffraction. A single crystal structure of FMT–MNBA (1:1) was successfully obtained, and then the solubility and permeability of the newly synthesized salt cocrystal were studied. The results showed that, compared with free FMT, the FMT from the FMT–MNBA cocrystal showed improved permeability. This study provides a synthetic method to improve the permeability of BCS III drugs, which will contribute to the development of low-permeability drugs.

1. Introduction

Clinically, many active pharmaceutical ingredients (APIs), especially in solid form, have low bioavailability due to their low solubility or poor permeability [1]. Synthesized salts, suitable solvates and cocrystal forms provide possibilities for solving the problems of solubility [2], permeability [3] and bioavailability [4] observed with APIs. For these formations, there is a necessary overlap between their definition as salts and as cocrystals; they are referred to as salt cocrystals here [5]. It has been reported that there is no covalent bond formation in the process of cocrystal formation. Therefore, without changing the physical and chemical properties of an API, the cocrystallization of the API with another bioacceptable molecule, namely, a cofomer (CCF), may improve some property defects of the API, such as stability [6], humidity [7], solubility [8], dissolution rate [9] and bioavailability [10,11]. In pharmaceutical science, rational selection of CCFs for a desired API is achieved through the identification of pharmaceutically relevant supramolecular synthons [12,13]. Although this method cannot completely predict cocrystal formation, it can provide a reasonable expectation. A crystal engineer can adopt any API and develop a cocrystallization strategy [14–16].

Famotidine (FMT) is a histamine H₂-receptor blocking agent that inhibits gastric acid secretion [17]. It is mainly used for the treatment of gastric and duodenal ulcers, reflux esophagitis, upper gastrointestinal bleeding and other gastrointestinal diseases. This API is also used clinically for the treatment of Zhuo-ai syndrome. M-nitrobenzoic acid (MNBA) was selected as CCF. Studies have

* Corresponding author. College of Pharmacy, Qingdao University, Qingdao, 266071, China.
E-mail address: yangzhaosyy@qd.shandong.cn (Z. Yang).

<https://doi.org/10.1016/j.heliyon.2023.e17494>

Received 3 June 2023; Received in revised form 16 June 2023; Accepted 20 June 2023

Available online 21 June 2023

2405-8440/© 2023 Published by Elsevier Ltd. This is an open access article under the CC BY-NC-ND license (<http://creativecommons.org/licenses/by-nc-nd/4.0/>).

shown that nitrobenzoic acid compounds have significant cytotoxic activities against a variety of tumors [18]. According to the Biopharmaceutics Classification System (BCS), FMT belongs to the BCS-III class of drugs, with poor permeability [19], oral absorption and bioavailability were seriously affected. Drug cocrystallization technology can provide a way to optimize the physicochemical and pharmacokinetic properties of FMT without changing the chemical structure or intrinsic biological activity of the API.

FMT comes in two crystal forms: type A and type B. Type B crystals are the first choice for commercial preparations because they have physical properties that enable them to have higher bioavailability [20]. However, type B is metastable form, so stability issues related to conversion to the more stable A form may arise during processing and storage. Polymorphism in FMT can be avoided via cocrystal formation with *p*-toluenesulfonic acid.

With crystal engineering, it is possible to obtain compounds with improved properties. In its structure, as shown in Fig. 1a, FMT has multiple sites with potential hydrogen-bonding abilities. Meanwhile, as shown in Fig. 1b, MNBA, an antitumor intermediate, contains a carboxyl group that is a potential candidate to participate in supramolecular isoacetylene with FMT. Therefore, MNBA was selected as the cofomer for this study.

The cocrystals of FMT obtained at present include: (1) cocrystals of famotidine–nicotinic acid (FMT–NIC) and famotidine–malonic acid (FMT–MAL), obtained by Zhang Yan et al. [21,22]; (2) famotidine–maleic acid (FMT–MLT), obtained by RUSSO et al. [20]. (3) famotidine–sorbic acid (FMT–FSOR) and famotidine–syringic acid (FMT–FSY), obtained by Akshita Jindal et al. [23]. The water solubility of the above FMT cocrystals has been greatly improved; however, FMT belongs to the BCS III class of drugs, and permeability is the biggest limitation of its bioavailability. The selected CCF MBNA has lower solubility than the previous CCF but has higher fat solubility, which can improve the permeability of FMT.

2. Materials and methods

2.1. Materials

FMT (drug substance, type B) was supplied by Qingdao Liteng Chemical Medical Research Co. Ltd. (Qingdao, China). MNBA was purchased from Aladdin. Acetonitrile was purchased from Merck (Darmstadt, Germany). Sodium acetate, glacial acetic acid, sodium dihydrogen phosphate and sodium hydroxide were purchased from Sinopharm Chemical Reagent Co. Ltd. (Shanghai, China).

3. Methods

3.1. Preparation of the salt cocrystal

The culture was carried out using the solvent evaporation method combined with ultrasound. FMT was dissolved in acetonitrile by ultrasound for over 1 h. After dissolution of FMT, MNBA was added and ultrasound continued for more than 1 h. The resulting solution was cooled to room temperature, filtered into a small beaker, and then sealed with a sealing film. After this, the film was punctured and the solution was allowed to slowly evaporate at room temperature. After 3–4 days, fine colorless needle crystals, suitable for single crystal X-ray diffraction, were obtained.

3.2. Scanning electron microscopy

Double-sided tape with the sample was fixed on an aluminum plate and coated with a platinum layer to make it conductive. The crystal morphologies of various samples were analyzed by scanning electron microscope (SEM) using a VEGA3 instrument (TESCAN, Czech Republic) under vacuum SEM at 20.0 kV.

3.3. Thermal analysis

Differential scanning calorimetry (DSC) was performed using a DSC 6000 instrument (PerkinElmer, Waltham, Massachusetts, USA). The samples were in an airtight pinprick aluminum pan, and the typical sample size was 3–5 mg. The samples were purged with a 20 mL/min flow of dry nitrogen. The heating rate was 20 °C/min and the temperature range was 30–250 °C.

Thermogravimetric analysis (TGA) was performed using a TGA 4000 instrument (PerkinElmer, Waltham, MA, USA). The samples were in an airtight pinprick aluminum pot, and the typical sample size was 5–12 mg. The samples were purged with a 20 mL/min flow of dry nitrogen. The heating rate was 20 °C/min and the temperature range was 30–350 °C.

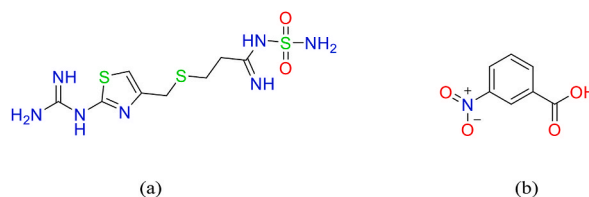


Fig. 1. (a) Chemical structures of famotidine (FMT), (b) *m*-nitrobenzoic acid (MNBA).

3.4. Powder X-ray diffraction

Powder X-ray diffraction (PXRD) was performed using a Bruker D8 Focus. The sample was placed in a small circular plate with a groove and then spread out and flattened. Cu- $\kappa\alpha$ radiation (1.54060 Å) was used, and the voltage and current were set at 40 kV and 40 mA, respectively. Data were collected at room temperature with a reflection mode range of 10–40° and a scanning speed of 2°/min.

3.5. Single crystal X-ray diffraction

A suitable crystal was selected and placed on an XtaLAB Synergy R, DW system HyPix diffractometer. A monochromatized Cu $\kappa\alpha$ (input = 1.54056 Å) ray was used with graphite at 293 (2) K at $7.54^\circ < 2\theta < 156.24^\circ$. Emission data were collected in $\omega/2\theta$ scanning mode.

3.6. Infrared spectra

Infrared spectra (FT-IR) analysis was performed using a Thermo Nicolet IS5 FT-IR spectrometer (Thermo Fisher Scientific). The typical sample concentration of 20 mg KBr was 2 mg, which was fully ground and then pressed. The infrared spectrum of the sample was collected using KBr diffuse reflection mode.

3.7. High-pressure liquid chromatography

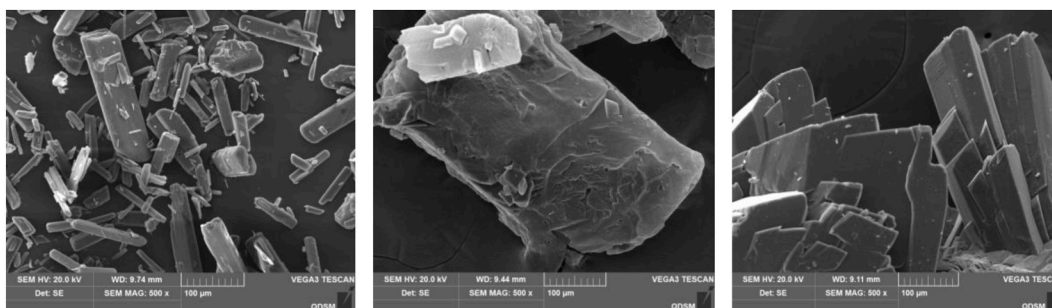
The properties of FMT were studied using an Agilent 1260 analyzer with a Capcell Pak MG-II C18 column (5 μm , 4.6 mm \times 250 mm). The mobile phase was acetate buffer solution–acetonitrile (93:7). The flow rate was 1.5 mL per min. The detection wavelength was 270 nm. Column temperature was 35 °C and sample volume was 20 μL . An appropriate amount of FMT standard was weighed and dissolved in a phosphate buffer solution as a reserve solution and standard curves in the range of 1.00–100.32 $\mu\text{g/mL}$ were constructed.

3.8. Equilibrium solubility

The equilibrium solubility of the FMT–MNBA salt cocrystals and the free API materials were determined using the shaking flask method. Excess FMT and FMT–MNBA were put into separate triangle bottles containing 10 mL water. The bottles were then plugged and placed in a constant temperature shaker (IKA KS 4000 I control) at a temperature of 25 °C. Appropriate samples of each type were taken at 4 h and 6 h. After filtration through a microporous membrane, a solvent phosphate was used to dilute to an appropriate concentration. The equilibrium solubility of FMT and FMT–MNBA were calculated using the HPLC method. Each sample was tested twice in parallel under the same conditions.

3.9. Permeability measurement

The permeation parameters of the FMT–MNBA salt cocrystal and its raw constituents were measured with a 96-well Permeapad® plate (LOGAN, Germany). The bottom layer was the recipient chamber with a 400 μL pH 7.4 phosphate buffer solution. The middle layer had a Permeapad® membrane (0.20 cm^2) and was the donor chamber with 50 μL water after adding an excess powder sample. The top layer was covered and sealed with sealing film. The entire unit was placed in a constant temperature shaker at 37 °C 200 rpm. The acceptor solution was replaced every hour with the same amount of fresh acceptor solution. After the experiment, the above liquid phase method was used for determination. For each sample, two measurements were made under the same conditions and the average value was calculated.



(a) (b) (c)

Fig. 2. SEM images of supplied (a) FMT, (b) MNBA and (c) FMT–MNBA salt cocrystal.

4. Results and discussion

4.1. Scanning electron microscope

Fig. 2 shows 500× SEM images of FMT, MNBA and FMT–MNBA. The grain size of FMT is uneven and its appearance is prismatic (Fig. 2a), the appearance of MNBA is sparsely lumpy and hollow (Fig. 2b), and the FMT–MNBA (1:1) is compact in appearance and consists of many smooth strips grouped into large lumps (Fig. 2c). These results suggest that the morphology of the salt cocrystal is different from that of FMT and MNBA, which indicates that the physical and chemical properties may have changed.

4.2. Thermal analysis

DSC is generally regarded as the first step in determining the formation of new crystalline phases. The newly formed salt cocrystal should have its own unique thermal behavior from both the API and the CCF [24]. Toward this end, the thermal behavior of the salt cocrystal was investigated using DSC as the first step to characterizing the new crystals.

As shown in Fig. 3, the DSC analysis of the FMT–MNBA salt cocrystal presents an endothermic event at about 173.67 °C, corresponding to the melting of the salt cocrystal. This new endothermic event is different from the melting points of FMT (171.70 °C) and MNBA (152.40 °C). This difference in timing suggests that the product is neither a single component nor a simple physical mixture; rather, it is a new substance that has its own unique melting point. These observations are bolstered by the following characterization analysis.

Used together to characterize crystals, TGA and DSC reveal the thermal behaviors of products. They not only verify the melting point peak by revealing a product's endothermic behavior in DSC, but also preliminarily indicate whether the product contains solvents, especially water molecules.

The black curve in Fig. 4 shows the TGA thermodynamic change of the FMT–MNBA salt cocrystal. The weight loss starts at about 197 °C, which is the beginning of the decomposition process after the melting point of the cocrystal (173.67 °C). In addition, there is no weight loss within or near 100 °C, indicating that the structure is without solvent or water molecules. This result is in agreement with the following single-crystal structure results.

4.3. Powder X-ray diffraction analyses

As a mature method of crystal characterization, PXRD is widely used to characterize the structure of crystalline materials [25]. It can provide important information about crystallization, purity and degree of crystallization.

As shown in Fig. 5, FMT–MNBA and the free APIs, FMT and MNBA, were tested by PXRD, and their diffraction patterns were recorded and described. Compared with the two constituents, the newly synthesized FMT–MNBA showed new sharp diffraction peaks at 2θ values of 13.44°, 20.60° and 25.81°, respectively. It is worth noting that these characteristic peaks were newly generated and were absent from the pure FMT and MNBA diffraction patterns. Moreover, the characteristic diffraction peaks of FMT (11.69°, 24.21° and 35.44°) and MNBA (13.93° and 23.30°) disappear in the diffraction pattern of FMT–MNBA, which confirms the emergence of a new crystal phase. This finding is consistent with the above DSC, TGA and IR results. In addition, it can also be seen from Fig. 8 that the matching degree between the tested PXRD model and the current standard PXRD model of FMT–MNBA is close to 100%, indicating that the powder samples prepared in this work have high purity and can be used as the test samples of FMT–MNBA in subsequent relevant experimental studies.

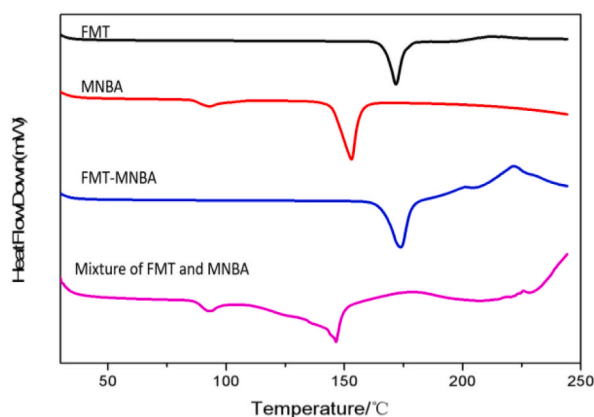


Fig. 3. DSC thermograms of FMT, MNBA, FMT–MNBA, FMT/MNBA.

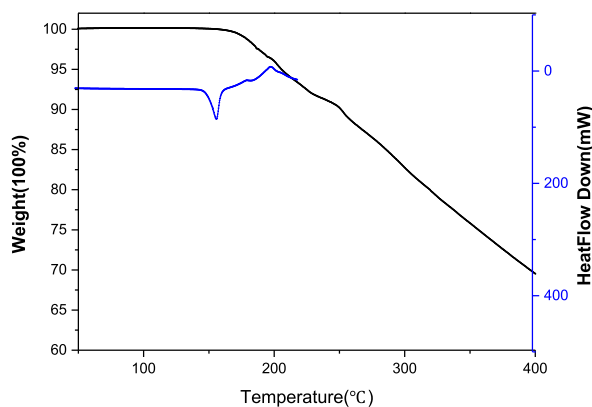


Fig. 4. DSC and TGA thermograms of FMT-MNBA.

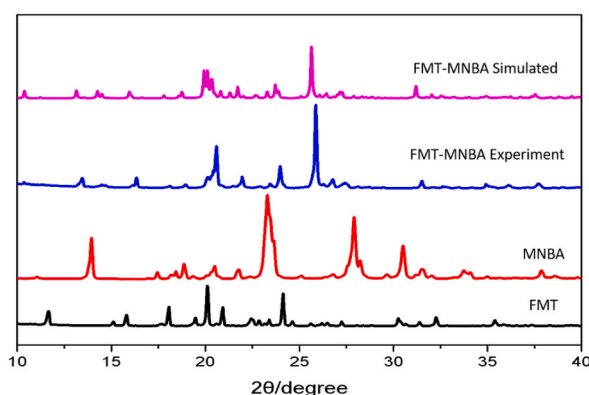


Fig. 5. PXRD patterns of FMT, MNBA and FMT-MNBA for both experimental and simulated.

4.4. Salt cocrystal structure

X-ray structure analysis revealed that the cocrystal belongs to the triclinic system of space group P-1. The new crystal's unit cell measurements and other relevant crystallographic parameters are summarized in Table 1.

As shown in Fig. 6, the asymmetric unit of FMT-MNBA consists of an FMT molecule and an MNBA molecule. An FMT-MNBA

Table 1
Crystallographic parameters of the FMT-MNBA cocrystal.

Empirical formula	C15H25N7O6S4
Formula weight	505.58
Temperature (K)	293 K
Wavelength (Å), Cu-K α	1.54184
Crystal system	triclinic
Space group	P1
a (Å)	8.78926 (14)
b (Å)	10.6575 (2)
c (Å)	12.9297 (2)
α (°)	69.3636 (16)
β (°)	76.3040 (14)
γ (°)	89.1726 (14)
Volume (Å ³)	1098.03 (4)
Z	2
F (000)	526.0
Crystal size (mm)	0.050 , 0.200 , 0.200
θ range for data collection (°)	3.770to78.124
Limiting indices	$-11 \leq h \leq 9, -16 \leq k \leq 15, -13 \leq l \leq 13$
R1, ω R2, S	0.0501 , 0.1316 , 1.072
Deposition number	2219775

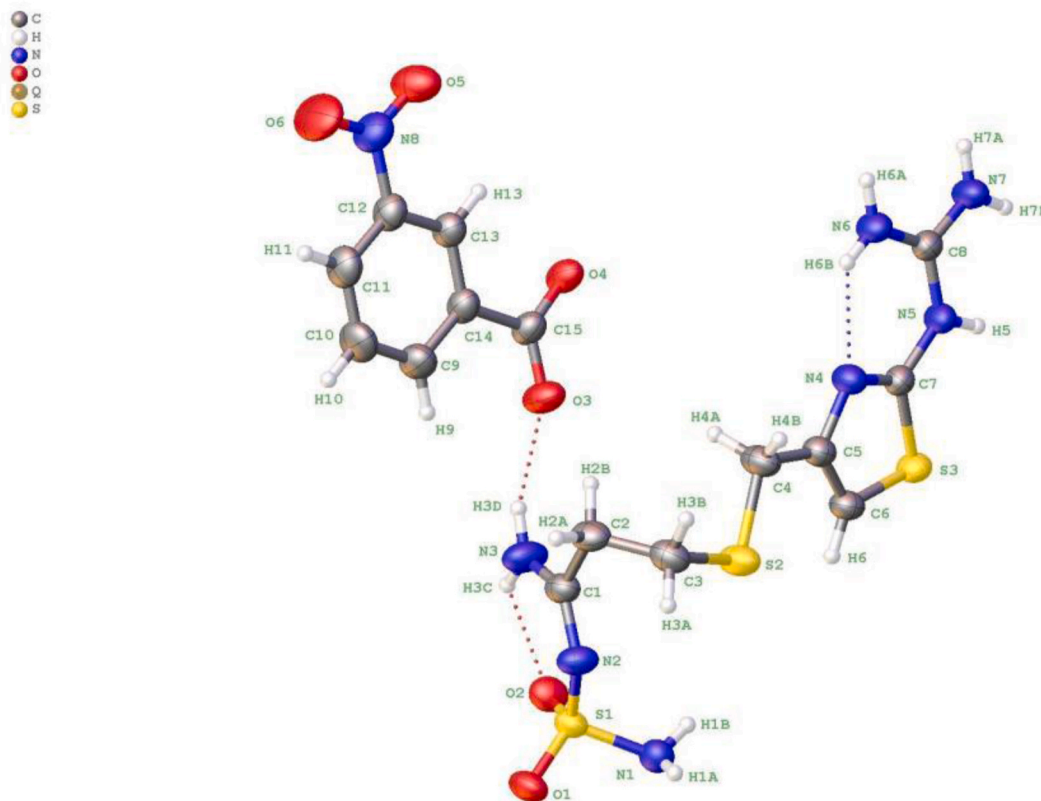


Fig. 6. Hydrogen bonds in FMT-MNBA.

structural unit consists of two types of hydrogen bonds. One bond is an intermolecular hydrogen bond that directly links the two molecules including N7–H7B...O3, N3–H3D ... O3, N1–H1A ... O4, N5–H5...O4; the other is the intermolecular hydrogen bond of FMT itself including N6–H6B...N4, N6–H6A ... O1, N3–H3C...O2. As shown in Fig. 7, the connections extend the stacks to form a supra-molecular stacking network structure. The crystallographic data in the form of CIF has been uploaded to the Cambridge crystal database center, deposition number 2219775.

It can be seen from the crystal structure (Figs. 6 and 7) that proton transfer occurred in the crystal. However, as seen in Table 2, the bond length is between 1.9 and 2.9 [26,27], which is in the range of a hydrogen bond. The crystal is defined as both a cocrystal and salt, and is therefore a salt cocrystal.

4.5. IR analyses

The infrared spectra of the free API and CCF and the salt cocrystal were collected in the range of 4000–400 cm^{-1} [28]. The wave number changes of different absorption peaks of the API and the CCF during salt cocrystal formation were preliminarily indicated, and the groups of hydrogen bonds formed by the X-ray single crystal diffraction were verified.

As shown in Fig. 8, the infrared absorption spectra of the FMT–MNBA and free FMT and MNBA materials were recorded. The absorption peaks of pure FMT at 3395 cm^{-1} and 1603 cm^{-1} correspond to the N–H vibration of guanidine. After the formation of FMT–MNBA, the maximum absorption peak at 3395 cm^{-1} shifted to 3353 cm^{-1} and the peak at 1603 cm^{-1} shifted to 1636 cm^{-1} . The maximum absorption peak of the MNBA at 1557 cm^{-1} was attributed to the stretching vibration of C=O. After the formation of FMT–MNBA, the maximum absorption peak at 1557 cm^{-1} shifted to 1552 cm^{-1} . A series of infrared peaks moved from 3395 cm^{-1} to 3353 cm^{-1} , from 1603 cm^{-1} to 1636 cm^{-1} , and from 1557 cm^{-1} to 1521 cm^{-1} , respectively. These changes were due to the formation of hydrogen bonds between the FMT and the MNBA.

4.6. Equilibrium solubility

The sample concentration of FMT, measured by HPLC was similar at 4 h and 6 h, indicating that the equilibrium of FMT, whether in salt cocrystal or free, had been reached at 4 h, and that solubility would no longer increase. The equilibrium solubility data of FMT and FMT–MNBA are shown in Table 3. The equilibrium solubility of free FMT in water at 25 °C was 0.77 mg/mL and the equilibrium solubility of FMT–MNBA was 0.84 mg/mL. In conclusion, the solubility of FMT increased by 1.09 times after salt cocrystal formation

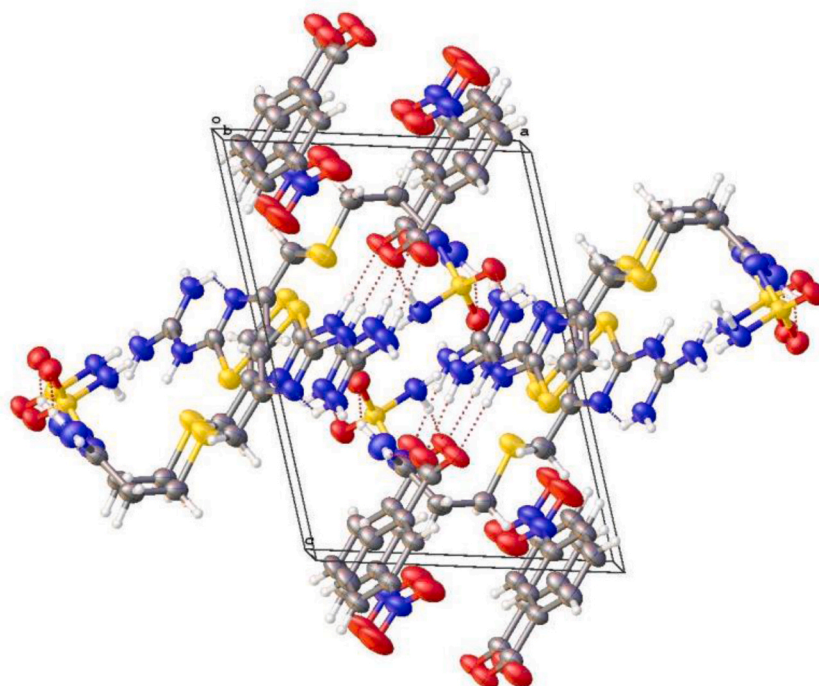


Fig. 7. View of the 3D supramolecular structure of FMT-MNBA.

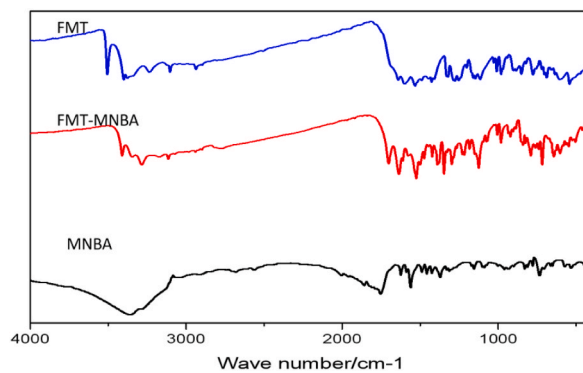


Fig. 8. IR spectra of the FMT, FMT-MNBA and MNBA.

Table 2

Hydrogen-bonding geometries of FMT-MNBA (Å, °).

D-H...A	d (D-A)	d (H...A)	∠D-H...A
N3-H3D ... O3	2.841	2.023	158.69
N6-H6A ... O1	2.984	2.133	170.69
N7-H7B...O3	2.778	1.919	177.276
N6-H6B...N4	2.719	2.070	131.626
N5-H5...O4	2.722	1.872	169.680
N1-H1A ... O4	2.922	2.060	163.828
N3-H3C...O2	2.758	2.155	126.875

Table 3
Equilibrium solubility results of FMT and FMT–MNBA.

Sample	Solubility mg.ml $-1 \pm$ SD	Increased solubility %
FMT	0.77	100.00
FMT–MNBA	0.84	109.09

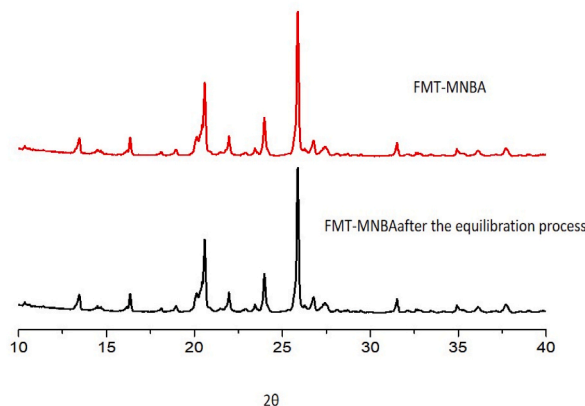


Fig. 9. PXRD patterns of FMT–MNBA and product after the equilibration process in water.

with MNBA. As shown in Fig. 9, undissolved FMT–MNBA samples were collected, and the results of the PXRD analysis were the same as those before the experiment.

From a structural point of view, the increase slightly in solubility in the salt cocrystal can be explained by the fact that when it was exposed to an aqueous environment, the MNBA molecules in the crystal, which have high solubility, are the first to be dissolved in the water. This leaves the FMT molecules from the crystal in an amorphous state in the aqueous solution. This amorphous state quickly dissipates and dissolves in the water of the aqueous solution. As a result of this process, the FMT from the salt cocrystal has a higher solubility than pure FMT API molecules [29]. In summary, the improvement in the water solubility of FMT is attributed to the high water solubility of MNBA.

4.7. Permeability studies

In vitro permeability measurement is usually performed by rat intestinal perfusion, biomimetic permeable membrane and Caco-2 cell tests [30,31]. The permeability study was performed using a Permeapad® plate [32], an artificial biomimetic membrane with a lamellar structure completely based on phospholipids. With Permeapad® permeability data obtained from optimization literature, the Caco-2 cell or the PAMPA methods measuring data have good correlation [32]. In this study, the experiment was carried out for 8 h, with the permeability of the drug through the whole membrane measured every hour to obtain the hourly permeability and total permeability of the free FMT and the FMT–MNBA salt cocrystal [33]. Figs. 10 and 11 show the hourly permeability and total permeability of the free FMT and FMT–MNBA salt cocrystal, respectively. From Fig. 10, FMT–MNBA is seen to have a higher hourly penetration than FMT. As can be seen from Fig. 11, the cumulative penetration amount of FMT–MNBA after 8 h is higher than that of free FMT. The total penetration of FMT–MNBA is about 1.75 times that of free FMT. These figures clearly show that cocrystallization enhances the penetration of FMT through artificial membranes compared to pure FMT.

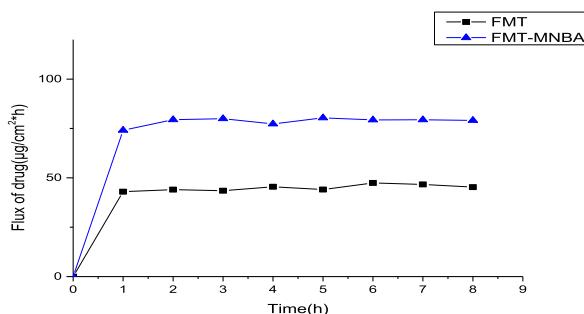


Fig. 10. FMT and FMT–MNBA salt cocrystal penetration per hour.

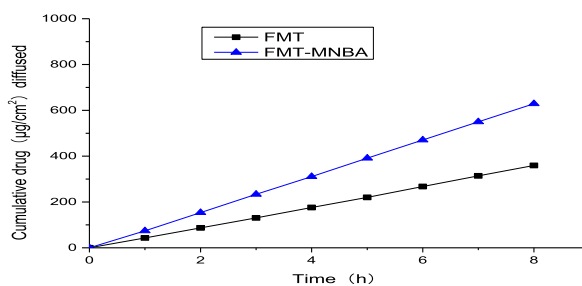


Fig. 11. FMT and FMT-MNBA salt cocrystal cumulative permeability.

This enhanced penetration may be by considering the following factors: On one hand, the excellent solubility of the salt cocrystal leads to a larger concentration gradient on the membrane, which can be used as a driving force to enhance the cocrystal's permeability. On the other hand, the increase in permeability may also be due to the greater lipophilicity of MNBA compared to FMT. As an important permeability evaluation parameter, the lipid-water distribution coefficient ($\log P$) has an important reference value for eutectic permeability [34]. Compared with FMT, MNBA has a higher $\log P$ value (1.8 vs. -0.4). Salt cocrystals utilize the permeability advantage of MNBA by assembling FMT-MNBA hydrogen bond clusters. Therefore, the permeability of FMT is improved by combining it with MNBA to pass through the non-polar membrane.

5. Conclusion

To improve the poor permeability of FMT, an FMT-MNBA salt cocrystal was synthesized using drug cocrystallization technology. The cocrystal was characterized via DSC, TGA, SEM, FT-IR and PXRD analyses and its crystal structure was obtained successfully by SXRD. FMT-MNBA consists of one molecule of FMT and one molecule of MNBA. In vitro property studies showed that the water solubility and permeability of FMTs increased by 1.09 and 1.75 times, respectively. The obtained salt cocrystal in this work is expected to improve the bioavailability of FMT, further experiments are needed to confirm it. This study provides a synthetic method to improve the permeability of BCS III drugs, which will contribute to the development of low-permeability drugs.

Author contribution statement

Yongfeng Zhao: Conceived and designed the experiments; Performed the experiments; Analyzed and interpreted the data; Wrote the paper.

Ying Fan; Hong Xu: Performed the experiments; Analyzed and interpreted the data; Wrote the paper.

Yan Zhang: Conceived and designed the experiments; Analyzed and interpreted the data; Wrote the paper.

Min Li: Conceived and designed the experiments; Performed the experiments; Analyzed and interpreted the data.

Yunjie Zhu: Analyzed and interpreted the data; Contributed reagents, materials, analysis tools or data; Wrote the paper.

Zhao Yang: Conceived and designed the experiments; Contributed reagents, materials, analysis tools or data; Wrote the paper.

Data availability statement

Data associated with this study has been deposited at Cambridge crystal database center under the accession number 2219775.

Additional information

No additional information is available for this paper.

Declaration of competing interest

The authors declare that they have no known competing financial interests or personal relationships that could have appeared to influence the work reported in this paper.

References

- [1] D.H. Leung, S. Lohani, R.G. Ball, et al., Two novel pharmaceutical cocrystals of a development compound – screening, scale-up, and characterization, *Cryst. Growth Des.* 12 (3) (2012) 1254–1262.
- [2] K. Sugandha, S. Kaity, S. Mukherjee, et al., Solubility enhancement of ezetimibe by a cocrystal engineering technique, *Cryst. Growth Des.* 14 (9) (2014) 4475–4487.
- [3] A.R. Ilie, B.T. Griffin, M. Brandl, et al., Exploring the impact of supersaturated lipid-based drug delivery systems of celecoxib on in vitro permeation across permeapad (R) membrane and in vivo absorption, *J. Pharm. Sci.* 152 (2020), 105452.
- [4] N.K. Duggirala, M.L. Perry, O. Almarsson, et al., Pharmaceutical cocrystals: along the path to improved medicines, *Chem. Commun.* 52 (4) (2015) 640–655.
- [5] C.C. Sun, Cocrystallization for successful drug delivery, *Expert Opin. Drug Discov.* 10 (2) (2013) 201–213.

- [6] Q.H. Yu, Z.C. Yan, J.J. Bao, et al., Taming photo-induced oxidation degradation of dihydropyridine drugs through cocrystallization, *Chem. Commun.* 53 (91) (2017) 12266–12269.
- [7] C.A. Gunawardana, C.B. Aakeroy, Co-crystal synthesis: fact, fancy, and great expectations, *Chem. Commun.* 54 (100) (2018) 14047–14060.
- [8] Q. Ning, M. Li, W. Schlindwein, et al., Pharmaceutical cocrystals: an overview, *Int. J. Pharm.* 419 (1–2) (2011) 1–11.
- [9] G. Bolla, A. Nangia, Pharmaceutical cocrystals: walking the talk, *Chem. Commun.* 52 (54) (2016) 8342–8360.
- [10] P.S. Panzade, G.R. Shendarkar, Pharmaceutical cocrystal: a game changing approach for the administration of old drugs in new crystalline form, *Drug Dev. Ind. Pharm.* 46 (10) (2020) 1559–1568.
- [11] S. Tothadi, G.R. Desiraju, Designing ternary cocrystals with hydrogen bonds and halogen bonds, *Chem. Commun.* 49 (71) (2013) 7791–7793.
- [12] M.G. Schmidt, Photodimerization in the solid state, *Pure Appl. Chem.* 27 (4) (1971).
- [13] M.C. Etter, Hydrogen bonds as design elements in organic chemistry, *J. Phys. Chem.* 95 (12) (1991) 4601–4610.
- [14] G.R. Desiraju, Supramolecular synthons in crystal engineering—a new organic synthesis, *Angew. Chem. Int. Ed.* 34 (21) (2010) 2311–2327.
- [15] C.B. Aaker, Y.D.J. Salmon, Building co-crystals with molecular sense and supramolecular sensibility, *CrystEngComm* 7 (72) (2005) 439–448.
- [16] S. Tothadi, G.R. Desiraju, Designing ternary cocrystals with hydrogen bonds and halogen bonds, *Chem. Commun.* 49 (71) (2013) 7791–7793.
- [17] R.W. Malone, More than just heartburn: does famotidine effectively treat patients with COVID-19? *Dig. Dis. Sci.* 66 (2021) 3672–3673.
- [18] Y.B. Zheng, J.H. Gong, Y.S. Zhen, et al., Application of Nitrobenzoic Acid Compounds in the Preparation of Drugs for the Treatment of Tumor, 2020. CN111297870A.
- [19] S.K. Jha, R. Karki, V.D. Puttegowda, et al., In vitro intestinal permeability studies and pharmacokinetic evaluation of famotidine microemulsion for oral delivery, *Int. Sch. Res. Notices* (2014), 452051.
- [20] M.G. Russo, E.V. Brusau, J. Ellena, et al., Solid-state supramolecular synthesis based on the N-H center dot center dot center dot O heterosynthon: an approach to solve the polymorphism problem in famotidine, *J. Pharm. Sci.* 103 (11) (2014) 3754–3763.
- [21] Y. Zhang, Z. Yang, S. Zhang, et al., Synthesis, crystal structure, and solubility analysis of a famotidine cocrystal, *Crystals* 9 (7) (2019) 360.
- [22] Y. Zhang, Y.P. Zhu, S.H. Zhang, et al., Study on improving the solubility of famotidine by cocrystal formation with niacin, *Chin. Pharmaceut. J.* 54 (13) (2019) 6.
- [23] J. Akshita, P. Mansi, D. Janhvi, et al., Pharmaceutical cocrystals of famotidine: structural and biopharmaceutical evaluation, *J. Pharm. Sci.* 111 (10) (2022) 2788–2798.
- [24] S.H. Zhang, Z. Yang, Y. Zhang, et al., Synthesis, characterization and physicochemical properties of an ibuprofen pharmaceutical cocrystal, *Struct. Chem.* (8) (2020) 1444–1450.
- [25] L. Min, Y. Zhao, Z. Yan, et al., Synthesis, crystal structure, and solubility study of a supramolecular assembly cocrystal formed by levofloxacin and nicotinic acid, *J. Mol. Struct.* (2022) 1249.
- [26] J.G. Sander, D.K. Bucar, R.F. Henry, et al., 'Masked synthons' in crystal engineering: insulated components in acetaminophen cocrystal hydrates, *CrystEngComm* 15 (24) (2013) 4816–4822.
- [27] F. Bruni, C.D. Mino, S. Imberti, et al., Hydrogen bond length as a key to understanding sweetness, *J. Phys. Chem. Lett.* 9 (13) (2018) 3667–3672.
- [28] E.Y. Tupikina, A.A. Titova, M.V. Kaplanskiy, et al., Estimations of OH-N hydrogen bond length from positions and intensities of IR bands, *Spectrochim. Acta. A Mol. Biomol. Spectrosc.* 275 (2022), 121172.
- [29] P. Sanphui, V.K. Devi, D. Clara, et al., Cocrystals of hydrochlorothiazide: solubility and diffusion/permeability enhancements through drug-coformer interactions, *Mol. Pharm.* 12 (5) (2015) 1615–1622.
- [30] M. Banik, S.P. Gopi, S. Ganguly, et al., Cocrystal and salt forms of furosemide: solubility and diffusion variations, *Cryst. Growth Des.* 16 (9) (2016) 5418–5428.
- [31] J.A. Christin, N. Sune, B. Martin, et al., Drug permeability profiling using the novel permeapad 96-well plate, *Pharm. Res. (N. Y.)* 37 (6) (2020) 93.
- [32] H.A. Bibi, R. Holm, A.B. Brandl, Use of Permeapad® for prediction of buccal absorption: a comparison to in vitro, ex vivo and in vivo method, *Eur. J. Pharmaceut. Sci.* 93 (2016) 399–404.
- [33] M. Tzanova, E. Randelov, P. Stein, et al., Towards a better mechanistic comprehension of drug permeation and absorption: introducing the diffusion-partitioning interplay, *Int. J. Pharm.* 608 (2021), 121116.
- [34] Q. Tao, Q.Q. Hao, A.P. Voronin, et al., Polymorphic forms of a molecular salt of phenazopyridine with 3,5-dihydroxybenzoic acid: crystal structures, theoretical calculations, thermodynamic stability, and solubility aspects, *Cryst. Growth Des.* 19 (10) (2019) 5636–5647.